

Shape-aware Feature Extraction for Instance Segmentation

Hao Ding, Siyuan Qiao, Wei Shen, Alan Yuille
Department of Computer Science, Johns Hopkins University

{hding15, siyuan.qiao, wshen10, alan.yuille}@jhu.edu

Abstract

Modern instance segmentation approaches mainly adopt a sequential paradigm - “detect then segment”, as popularized by Mask R-CNN, which have achieved considerable progress. However, they usually struggle to segment huddled instances, i.e., instances which are crowded together. The essential reason is the detection step is only learned under box-level supervision. Without the guidance from the mask-level supervision, the features extracted from the regions containing huddled instances are noisy and ambiguous, which makes the detection problem ill-posed. To address this issue, we propose a new region-of-interest (RoI) feature extraction strategy, named Shape-aware RoIAlign, which focuses feature extraction within a region aligned well with the shape of the instance-of-interest rather than a rectangular RoI. We instantiate Shape-aware RoIAlign by introducing a novel refining module built upon Mask R-CNN, which takes the mask predicted by Mask R-CNN as the region to guide the computation of Shape-aware RoIAlign. Based on the RoI features re-computed by Shape-aware RoIAlign, the refining module updates the bounding box as well as the mask predicted by Mask R-CNN. Experimental results show that the refining module equipped with Shape-aware RoIAlign achieves consistent and remarkable improvements than Mask R-CNN models with different backbones, respectively, on the challenging COCO dataset. The code will be released.

1. Introduction

Instance segmentation [1, 32, 33, 16, 10], an increasingly active research topic in recent years, is a combination of the elements from two classical computer vision tasks - object detection [14, 15, 35, 27, 34, 13, 23] and semantic segmentation [28, 8, 41, 40, 29]. It is challenging since it requires not only classifying and localizing all the object instances correctly in an image, but providing a precise segmentation mask for each instance at the same time.

Modern instance segmentation approaches are dominated by the paradigm - “detect then segment”, as popular-

ized by Mask R-CNN [18], which first detects object bounding boxes from rectangular region-of-interests (RoIs) and then segments object masks guided by the bounding boxes. This sequential process implies that mask prediction can be benefited from precise object bounding box detection. This motivates us to think about an opposite direction: *Can object bounding box detection take advantage of mask prediction?* Theoretically, the answer is positive, since, from the supervised learning perspective, mask-level supervision is more informative than box-level supervision. However, this direction has not been explored for instance segmentation due to the limit of the paradigm. Current methods, e.g., Mask R-CNN [18] and its variants [19, 26], directly take the off-the-shelf object detector, such as Faster R-CNN [35], trained only by box-level supervision.

The lack of mask-level supervision in object bounding box detection may result in two types of problems, when object instances are very close to each other. The first one is the ill-posed training problem, which is illustrated in Fig. 1. The red boxes are the generated RoIs, located in the middle of the two objects, serving as the references to perform object detection. The blue boxes are the ground-truth bounding boxes. As shown in Fig. 1 (a), a dog and a cat are in close proximity to each other, and the two class labels, “dog” and “cat”, are assigned to “RoI 1” and “RoI 2”, respectively, according to the commonly used intersection-over-union (IoU) threshold, i.e., 0.5. Despite being labeled differently, these 2 RoIs will have nearly the same features if current RoI feature extraction strategies are used, e.g., RoIPooling [35] and RoIAlign [18], which aggregate features over all the points within the rectangular RoIs. This leads to an ill-posed classification problem: the same features are mapped to different labels. Fig. 1 (b) depicts a similar case, but for bounding box regression. “RoI 1” and “RoI 2” also have very similar RoI features, but correspond to different regression targets.

The second type is the noisy ROI feature problem. An instance-of-interest can have an arbitrary shape, which may not be covered by a RoI tightly, and thus the feature points within this RoI may correspond to background or other instances. Consequently, the extracted ROI features may be

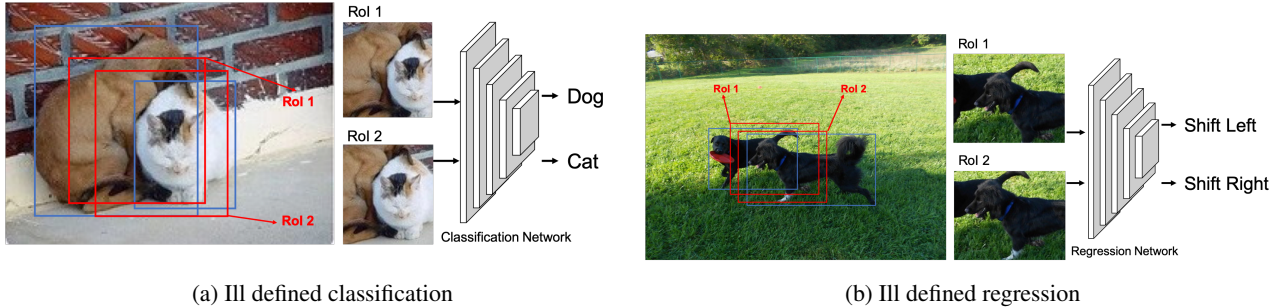


Figure 1: The ill-posed training problem caused by two huddled instances. The red boxes and blue boxes represent the generated RoIs and ground-truth bounding boxes, respectively. (a) Two highly similar RoIs are assigned with two different class labels. (b) Two highly similar RoIs are assigned with two different bounding box regression targets.

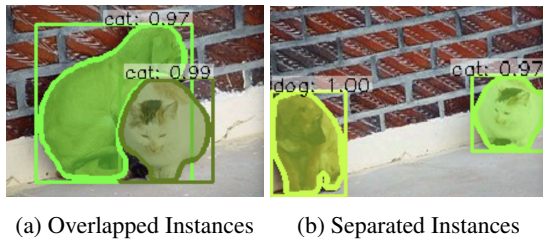


Figure 2: The noisy ROI feature problem. (a) A dog is misclassified as a cat, when a cat is in close proximity to it. (b) Both the cat and the dog are correctly classified when they are not close to each other.

noisy, and sometimes the noise is even stronger than the signal, *i.e.*, the activation values of the feature points corresponding to other instances are larger than those corresponding to the instance-of-interest. In this case, classification results based on the ROI features are prone to be wrong. As shown in Fig. 2, Mask R-CNN correctly classifies and segments a dog and a cat when they are not close to each other, but misclassifies the dog as a cat when the bounding box of the dog includes a large part of the cat.

To alleviate these two types of problems, we propose a mask guided ROI feature extraction strategy, Shape-aware RoIAlign, which implicitly imposes mask-level supervision to guide ROI feature extraction for bounding box detection. Shape-aware RoIAlign focuses feature extraction within a region aligned well with the shape of the instance-of-interest rather than a rectangular ROI. In this way, the noisy features from other instances and background are suppressed, and the ROI features of “RoI 1” and “RoI 2” in Fig. 1 become different. Ideally, the region should be the segmentation mask of the object, but it is unknown during inference. To realize Shape-aware RoIAlign, we design a novel refining module built upon Mask R-CNN, which takes

the mask predicted by Mask R-CNN as the region to guide the computation of Shape-aware RoIAlign. Based on the ROI features re-computed by Shape-aware RoIAlign, the refining module updates the predicted bounding box as well as the predicted mask. We refer to this method as MR R-CNN, for Mask Refining R-CNN.

Mask Refining R-CNN is easy to implement and can be trained end-to-end. Without bells and whistles, it consistently outperform the strong Mask R-CNN baseline by 1.5 box AP and 1.1 mask AP on the validation set of COCO 2017, as well as, 1.6 box AP and 1.0 mask AP on the test-dev set of COCO 2017.

Our main contributions are two-fold: (1) We propose Shape-aware RoIAlign, a mask guided ROI feature extraction strategy, which explicitly addresses the noisy ROI feature problem and the ill-posed training problem caused by huddled instances. (2) We realize Shape-aware RoIAlign in a new framework, MR R-CNN, which extends Mask R-CNN by adding a refining module for updating predictions based on the ROI features re-computed by Shape-aware RoIAlign. It consistently outperforms Mask R-CNN under different setups, *e.g.*, datasets and networks backbones.

2. Related Work

Since instance segmentation combines the elements from both object detection and semantic segmentation, existing methods for this task can be roughly categorized into two types: segmentation-based and detection-based.

2.1. Segmentation-based Methods

Segmentation-based methods usually adopt a two-step paradigm - “segment then identify”, *i.e.*, first perform semantic segmentation to obtain a per-pixel category-level segmentation map for an image, and then identify each object instance therefrom. Liang *et al.* [22] proposed to identify object instances from the segmentation map by spectral clustering. Kirillov *et al.* [20] partitioned instances from

the segmentation map with the help of a learned instance-wise edge map under a MultiCut formulation. Arnab and Torr [2] made use of the cues from the output of an object detector to identify instances from the segmentation map. Zhang *et al.* [39] predicted instance labels for local patches and merged similar predictions via a Markov Random Field (MRF). They then improved this method by using a densely connected MRF instead, which exploits fast inference [38]. Wu *et al.* [36] proposed a Hough-like Transform to bridge category-level and instance level segmentation, while Bai and Urtasun [3] achieved this by Watershed Transform. There are also some other methods which form instances from a segmentation map by learning an embedding to group similar pixels [31, 17, 30]. Liu *et al.* [25] proposed that the grouping problem can be broken into a series of sub-grouping problems and addressed sequentially.

2.2. Detection-based Methods

Detection-based methods first generate candidate bounding boxes, then segment the instance mask from each of them. Depending on how to generate the candidate bounding boxes, detection-based methods can be categorized into two classes: anchor-free and anchor-based.

Anchor-free methods. The early work of anchor-free methods directly used dense sliding-windows as the candidate bounding boxes, such as DeepMask [32], SharpMask [33] and InstanceFCN [11], which applied convolutional neural networks to predicting object masks in a dense sliding-window manner. Recent anchor-free methods design more sophisticated to generate mask proposals. YOLACT [4] first learned a dictionary of mask prototypes, and then predicted per-instance coefficients to linearly combine prototypes to produce an instance mask. ExtremeNet [42] used keypoint detection to predict extreme points, which provide an octagonal approximation for an instance mask. PolarMask [37] built a polar representation for each instance mask and formulated instance segmentation as instance center classification and dense distance regression in a polar coordinate. TensorMask [9] revisited the paradigm of dense sliding window instance segmentation and represented masks by structured 4D tensors over a spatial domain.

Anchor-based methods. Anchor-based methods take anchors as references to predict region proposals as the candidate bounding boxes, and then segment each instance mask using the box as a guide [21, 7]. This paradigm is known as “detect then segment”, which is currently the dominant paradigm. Mask-RCNN is a representative instantiation of this paradigm, which extended the well known anchor-based object detector, Faster R-CNN [35], with a mask segmentation branch. Follow-up works, i.e., the variants

of Mask-RCNN, improve it by enhancing feature pyramid with accurate localization signals existing in low-level layers [26], or re-scoring the confidence of a predicted mask by the Intersection-over-Union (IoU) between the mask and its ground-truth, to calibrates the misalignment between the mask score and its localization accuracy [19].

Current state-of-the-art instance segmentation method is HTC [6], which is a multi-stage framework by stacking Mask R-CNN in a cascaded structure [5]. It delivers the message that the mask prediction branch can be benefited from the updated bounding box regression. Our method, MR R-CNN, shows an orthogonal direction to the message given by HTC: the object detection branch, *i.e.*, object classification and bounding box regression, can take advantage of the updated mask predictions.

3. Methodology

In this section, we first describe our new RoI feature extraction strategy, Shape-aware RoIAlign, then introduce the architecture of MR R-CNN, to show how Shape-aware RoIAlign is applied to re-compute RoI features for updating predictions.

3.1. Shape-aware RoIAlign

We start this section by introducing RoIAlign [18], which is the standard operation used in Mask R-CNN for extracting features from an rectangular RoI. Given a feature map \mathcal{F} generated by a backbone network, it extracts a small feature map $\mathcal{F}_{\mathcal{R}}$ from a RoI \mathcal{R} by re-pooling the features in \mathcal{F} . The detail of this feature extraction procedure is described as below.

RoIAlign As shown in Fig. 3, RoIAlign uniformly divides the RoI \mathcal{R} into $H \times W$ bins. Each bin is denoted by $B_{h,w} = \{(x_h^1, y_w^1), (x_h^2, y_w^2)\}$, where (x_h^1, y_w^1) , (x_h^2, y_w^2) are the continuous coordinates of the top-left and bottom-right points of the bin at the h^{th} row and w^{th} column, respectively.

It then extracts a feature representation $\mathcal{F}_{\mathcal{R}}(w, h)$ for each bin $B_{h,w}$. Towards this end, N sampling points at continuous location $\{(a_{w,h}^i, b_{w,h}^i)\}_{i=1}^N$ are located uniformly within this bin $B_{w,h}$ for feature extraction. Given a sampling point (a, b) , the feature $f(a, b)$ at it is computed by bi-linear interpolation:

$$f(a, b) = \sum_{j,k} \omega(a, b, j, k) \times \mathcal{F}(j, k), \quad (1)$$

where $\omega(a, b, j, k) = \max(0, 1 - |a - j|) \times \max(0, 1 - |b - k|)$ represents the bi-linear interpolation coefficient and $\mathcal{F}(j, k)$ denotes the feature at a discrete location (j, k) on the feature map \mathcal{F} . Then the feature representation $\mathcal{F}_{\mathcal{R}}(h, w)$ for this bin $B_{h,w}$ is obtained by av-

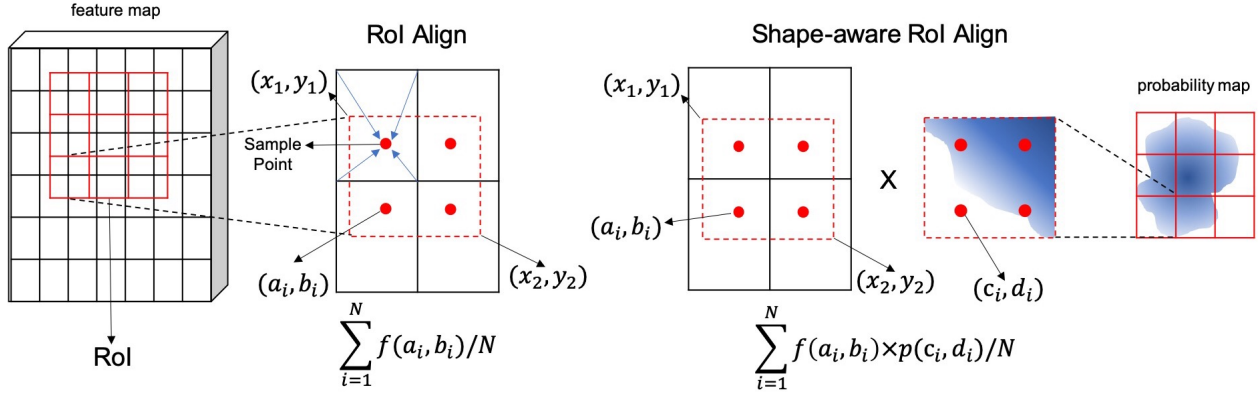


Figure 3: The illustration of RoIAlign and Shape-aware RoIAlign. In the illustration, a RoI is divided into 3×3 bins. For each bin, 4 sampling points are assigned (marked by red dots). The feature value of a sampling point is a bi-linear interpolation of its nearby feature values. RoIAlign averages the feature values at all sampling points, while Shape-aware RoIAlign uses a probability map of the instance-of-interest of the RoI to guide feature extraction.

eraging the features computed at all the sampling points $\{(a_{h,w}^i, b_{h,w}^i)\}_{i=1}^N$:

$$\mathcal{F}_{\mathcal{R}}(h, w) = \sum_{i=1}^N \frac{f(a_{h,w}^i, b_{h,w}^i)}{N}. \quad (2)$$

Finally, we collect the feature representations of all the bins and rearrange them to be the small feature map $\mathcal{F}_{\mathcal{R}}$. We denote this feature extraction procedure by a function $\mathcal{F}_{\mathcal{R}} = \text{RoIAlign}(\mathcal{R}, \mathcal{F})$ with the inputs \mathcal{R}, \mathcal{F} and the output $\mathcal{F}_{\mathcal{R}}$.

Shape-aware RoIAlign Shape-aware RoIAlign adds probability guidance to RoIAlign. It computes the feature values under the guidance of the probability of being the instance-of-interest at each locations. Similar to RoIAlign, it first divides a RoI \mathcal{R} into $H \times W$ bins, where each bin $B_{h,w}$ has N sampling points at continuous location $\{(a_{h,w}^i, b_{h,w}^i)\}_{i=1}^N$.

Then, given an additional $H_p \times W_p$ probability map \mathcal{P} aligned with the RoI \mathcal{R} , where each element $\mathcal{P}(j, k)$ denotes the probability of being the instance-of-interest at a discrete location (j, k) , we can have the probability $p(c, d)$ for any continuous coordinates (c, d) by bi-linear interpolation:

$$p(c, d) = \sum_{j,k} \omega(c, d, j, k) \times \mathcal{P}(j, k), \quad (3)$$

where $\omega(c, d, j, k)$ is the bi-linear interpolation coefficient. The feature representation $\mathcal{F}_{\mathcal{R}, \mathcal{P}}(h, w)$ of a bin $B_{h,w}$ is obtained by averaging the multiplications between feature values and probability values at the same sampling points:

$$\mathcal{F}_{\mathcal{R}, \mathcal{P}}(h, w) = \sum_{i=1}^N \frac{f(a_{h,w}^i, b_{h,w}^i) \times p(c_{h,w}^i, d_{h,w}^i)}{N} \quad (4)$$

where $(c_{h,w}^i, d_{h,w}^i)$ is the location at probability map \mathcal{P} corresponding to the location $(a_{h,w}^i, b_{h,w}^i)$ at feature map \mathcal{F} , which is obtained by:

$$\begin{aligned} c_{h,w}^i &= (a_{h,w}^i - x_0^1) \times \frac{H_p}{H} \\ d_{h,w}^i &= (b_{h,w}^i - y_0^1) \times \frac{W_p}{W} \end{aligned} \quad (5)$$

Finally, we obtain the small feature map $\mathcal{F}_{\mathcal{R}, \mathcal{P}}$ by repeating the above computation for each bin. We denote this feature extraction procedure, Shape-aware RoIAlign, by a function $\mathcal{F}_{\mathcal{R}, \mathcal{P}} = \text{SaRoIAlign}(\mathcal{R}, \mathcal{F}, \mathcal{P})$, with the inputs $\mathcal{R}, \mathcal{F}, \mathcal{P}$ and the output $\mathcal{F}_{\mathcal{R}, \mathcal{P}}$.

3.2. Mask Refining R-CNN

Now, only one problem remains: how to obtain the probability map \mathcal{P} as the input of the function SaRoIAlign ? Intuitively, this probability map \mathcal{P} is exactly the output of Mask R-CNN. Thus, we realize Shape-aware RoIAlign by building a refining module upon Mask R-CNN. The overall architecture is shown in Fig. 4, which is called Mask Refining R-CNN (MR R-CNN). The refining module takes the box prediction and mask prediction outputted by Mask R-CNN as its input, extracts RoI features by Shape-aware RoIAlign and refines box prediction and mask prediction by a refining box head and a refining mask head, respectively.

Vanilla Mask R-CNN. The vanilla Mask R-CNN consists of a backbone Network, a Region Proposal Network (RPN), a box head and a mask head. Given an input image, the backbone network generates a feature map \mathcal{F} from the image and the RPN generates a set of RoIs.

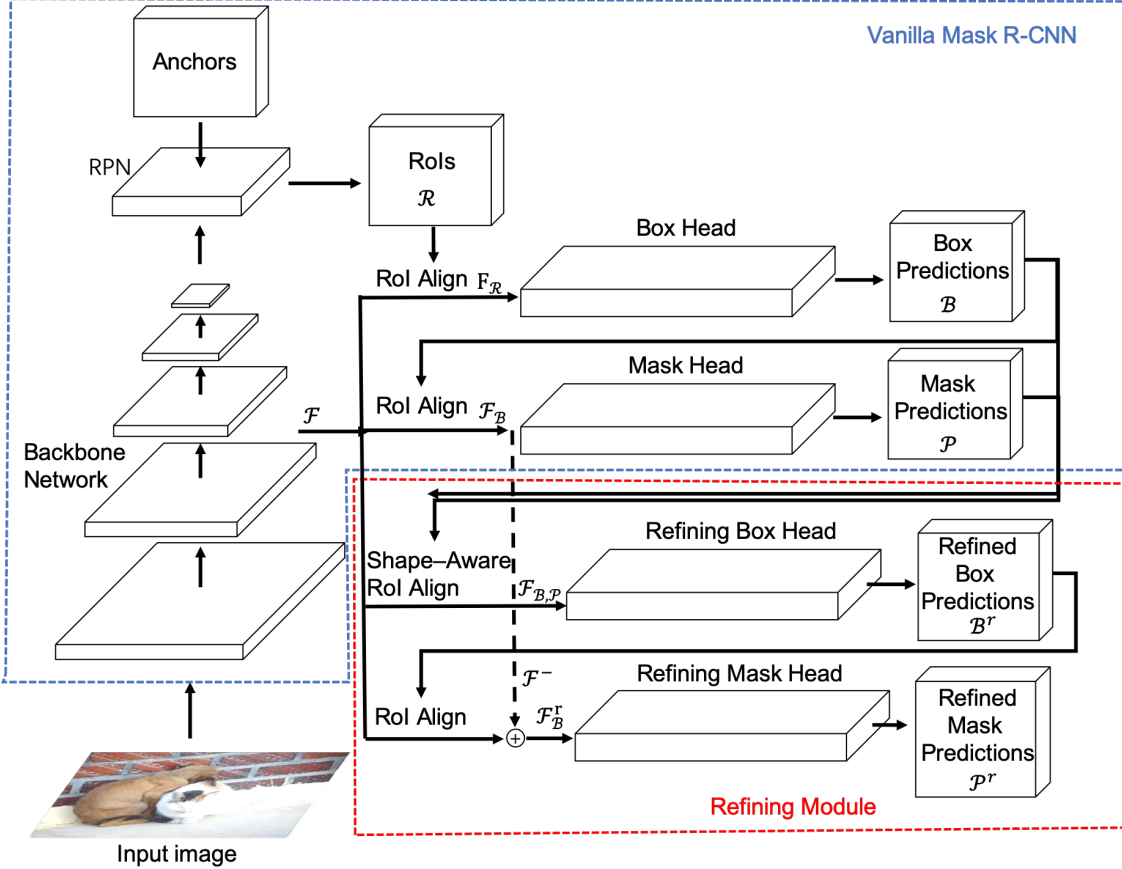


Figure 4: The network architecture of MR R-CNN, which consists of a vanilla Mask R-CNN model (bounded in the grey dashed line) and a refining module (bounded in the red dashed line). The refining module takes the box prediction, mask prediction and an intermediate mask feature from the Vanilla Mask R-CNN as its input, extracts RoI features by Shape-aware RoIAlign, and refines box and mask predictions as its output.

The box head takes each RoI \mathcal{R} as the reference, to compute the RoI feature representation by RoIAlign $\mathcal{F}_{\mathcal{R}} = \text{RoIAlign}(\mathcal{R}, \mathcal{F})$ and predict a bounding box \mathcal{B} of the instance-of-interest based on the RoI feature representation $\mathcal{F}_{\mathcal{R}}$. We denote this box prediction procedure by a function: $\mathcal{B} = \text{BoxHead}(\mathcal{F}_{\mathcal{R}}, \mathcal{R})$. The bounding box \mathcal{B} is also a rectangular region, *i.e.*, a RoI, which is then used for mask prediction. We denote the mask prediction procedure by a similar function: $\mathcal{P} = \text{MaskHead}(\mathcal{F}_{\mathcal{B}}, \mathcal{B})$, where $\mathcal{F}_{\mathcal{B}} = \text{RoIAlign}(\mathcal{B}, \mathcal{F})$. The mask prediction \mathcal{P} is a probability map for the instance-of-interest.

3.3. Mask Refining R-CNN

Refining module. The refining module consists of a refining box head and a refining mask head.

The refining box head takes the feature map \mathcal{F} , the bounding box \mathcal{B} and the probability map \mathcal{P} for the instance-of-interest obtained by the Vanilla Mask R-CNN

as its inputs. It first computes the RoI feature representation for \mathcal{B} by Shape-aware RoIAlign: $\mathcal{F}_{\mathcal{B}, \mathcal{P}} = \text{SaRoIAlign}(\mathcal{B}, \mathcal{P}, \mathcal{F})$, with the help of \mathcal{P} . Based on $\mathcal{F}_{\mathcal{B}, \mathcal{P}}$, the refining box head predicts a refined box \mathcal{B}^r . We denote this bounding box prediction procedure in the refining module by a function: $\mathcal{B}^r = \text{rBoxHead}(\mathcal{F}_{\mathcal{B}, \mathcal{P}}, \mathcal{B})$

We borrow the mask information flow strategy introduced in [6] to design the refining mask head. The principle of this strategy is the mask features of the refining stage can be enhanced by fusing with the mask features of the preceding stage. To this end, we extract an intermediate feature representation \mathcal{F}^- from the mask head of the the Vanilla Mask R-CNN. To obtain \mathcal{F}^- , we first feed $\mathcal{F}_{\mathcal{B}}$ into the first four consecutive 3×3 convolutional layers of the mask head, followed by a 1×1 convolutional layer to align the output \mathcal{F}^- with the same size as $\mathcal{F}_{\mathcal{B}}$.

Then the input feature $\mathcal{F}_{\mathcal{B}}^r$ for the refining mask head is obtained by the element-wise sum of the RoI feature repre-

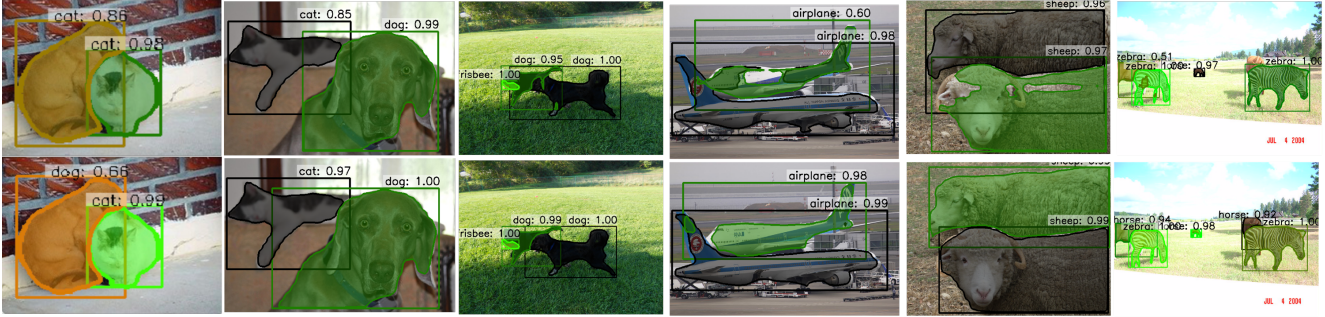


Figure 5: Qualitative comparison between Mask R-CNN (top) and MR R-CNN (bottom).

sensation for the bounding box \mathcal{B}^r and intermediate feature representation \mathcal{F}^- :

$$\mathcal{F}_B^r = \text{RoIAlign}(\mathcal{B}^r, \mathcal{F}) + \mathcal{F}^-. \quad (6)$$

Note that, we do not use Shape-aware RoIAlign to compute the RoI feature representation for mask segmentation, because 1) mask segmentation is guided by per-pixel labels, then does not suffer from the ill-posed training problem which box detection has, and 2) mask segmentation requires more image context than box detection.

Based on \mathcal{F}_B^r , the refining mask head predicts a refined Mask \mathcal{P}^r . This mask refinement procedure is denoted by a function: $\mathcal{P}^r = \text{rMaskHead}(\mathcal{F}_B^r, \mathcal{B}^r)$.

Training. The training strategy for our Mask refining R-CNN is not trivial. The mask head of the vanilla Mask R-CNN is only trained on foreground classes, which means it only generates mask predictions for RoIs with foreground class labels. As result, there will be no mask guidance for RoIs with the background class label, which leads to a bias in training.

To address this issue, we assign pseudo foreground labels to the RoIs with the background class label during training. The pseudo foreground label for a RoI with the background class label is the label of the foreground class with the largest classification score. The mask probability map corresponding to the assigned pseudo foreground label is then used for the mask guidance for the RoI. In this way, RoIs of both background and foreground class labels can be used to train a refining module.

Inference. During inference, we compute the weighted average of the classification score \mathcal{S}^b , i.e., the activation value before the softmax layer, given by the box head of the vanilla Mask R-CNN and the classification score \mathcal{S}^r given by the refining box head as the final classification score \mathcal{S} outputted by our MR R-CNN. This is formulated by $\mathcal{S} = \frac{\mathcal{S}^b + \alpha \times \mathcal{S}^r}{1 + \alpha}$, where α denotes the relative weight for

\mathcal{S}^r . The final bounding box prediction and mask prediction outputted by our MR R-CNN are \mathcal{B}^r and \mathcal{P}^r , respectively.

4. Experiment Result

All experiments are evaluated on MS-COCO 2017 dataset [24], which contains about 118k images with corresponding annotations as training set and 5k held-out images with annotations as validation set. The main metric used for evaluation is Average Precision (AP) averaged across IoU thresholds from 0.5 to 0.95 with 0.05 as interval. Our models are trained on 118k training set. Results on the held-out 5k validation set and 20k test-dev set are reported.

4.1. Implementation Details

Training: We take a pre-trained vanilla Mask R-CNN, build our refining module upon it, and initialize the refining module with the parameters in the heads of the pre-trained Mask R-CNN.

The model is trained on 4 GPUs with batch size 16 for 9k iterations with a starting learning rate of 0.002, which is multiplied by 0.1 at iteration 6k. The optimizer is SGD with a weight decay of 0.0001 and momentum of 0.9.

Inference: At inference time, we use standard non-maximum suppression algorithm with a threshold of 0.5 for duplicate removal. The weight α for combining the two classification scores is set to 1.0 as default.

4.2. Benchmarking Results

We first conduct an experiment on the validation set of COCO 2017 to show the improvement of our MR R-CNN to the strong baseline Mask R-CNN. We use ResNet-50 + FPN, ResNet-101 + FPN, ResNeXt-101-32x8d + FPN as the backbones. The results are shown in Table 1. AP_b denotes the average precision of bounding boxes results. AP_m denotes the average precision for segmentation results. The numbers behind AP_b and AP_m denote the IoU thresholds which the average precision values are computed at. The results of AP_b and AP_m show remarkable improvements,

Method	Backbone	AP_b	AP_{b50}	AP_{b75}	AP_m	AP_{m50}	AP_{m75}
Mask R-CNN	ResNet-50 FPN	37.8	59.1	41.0	34.2	55.6	36.5
MR R-CNN	ResNet-50 FPN	39.5	60.3	43.2	35.4	57.0	37.7
Mask R-CNN	ResNet-101 FPN	40.1	61.8	44.0	36.1	58.2	38.3
MR R-CNN	ResNet-101 FPN	41.4	62.4	45.5	37.1	59.1	39.7
Mask R-CNN	ResNeXt-101 FPN	42.2	64.0	46.1	37.8	60.6	40.2
MR R-CNN	ResNeXt-101 FPN	43.6	64.6	47.9	38.8	61.4	41.5

Table 1: Comparison to Mask R-CNN under different backbones on COCO 2017 validation set.

Method	Backbone	AP_b	AP_{b50}	AP_{b75}	AP_m	AP_{m50}	AP_{m75}
MNC[12]	ResNet-101	-	-	-	24.6	44.3	24.8
FCIS[21]	ResNet-101	-	-	-	29.2	49.5	-
FCIS++[21]	ResNet-101	-	-	-	33.6	54.5	-
MaskLab[7]	ResNet-101	-	-	-	35.4	57.4	37.4
MaskLab+[7]	ResNet-101	-	-	-	37.3	59.8	36.6
MaskLab+[7]	ResNet-101(JET)	-	-	-	38.1	61.1	40.4
MS R-CNN[19]	ResNet-101	39.1	58.2	43.2	35.4	54.9	38.1
MS R-CNN[19]	ResNet-101 FPN	41.6	62.3	46.2	37.4	57.9	40.4
MS R-CNN[19]	ResNet-101 DCN+FPN	43.6	64.4	48.5	39.6	60.7	43.1
Mask R-CNN[18]	ResNet-50 FPN	38.0	59.7	41.5	34.6	56.5	36.6
MR R-CNN	ResNet-50 FPN	39.9	60.9	43.5	35.6	57.7	38.0
Mask R-CNN[18]	ResNet-101 FPN	40.2	61.9	44.0	36.2	58.6	38.5
MR R-CNN	ResNet-101 FPN	41.5	62.8	45.4	37.2	59.7	39.7
Mask R-CNN[18]	ResNeXt-101 FPN	42.6	64.9	46.6	38.3	61.6	40.8
MR R-CNN	ResNeXt-101 FPN	44.1	65.7	48.3	39.3	62.6	42.0
MR R-CNN	ResNet-101 DCN+FPN	44.1	65.5	48.2	39.7	62.6	42.7

Table 2: Comparison between different instance segmentation methods on COCO 2017 test-dev.

i.e., 1.5 AP on average for bounding box detection and 1.1 AP on average for mask segmentation.

We then do comparison with some state-of-the-art instance segmentation methods on the test-dev set of COCO 2017. The results are shown in Table 2. We observe that MR R-CNN consistently achieves improvements to Mask RCNN, i.e., 1.6 AP on average for bounding box detection and 1.0 AP for mask segmentation, and outperforms other state-of-the-arts.

It is worth mentioning that the our method is complementary to these state-of-the-art methods, since we search an orthogonal direction, i.e., bounding box detection can take advantage of mask prediction.

Fig. 5 shows the qualitative comparisons between Mask R-CNN and MR R-CNN. We select the cases where the images contain huddled instances to demonstrate the motivation of Shape-aware RoIAlign and how well our proposed method is able to address the problems that exist for huddled instances as discussed in the introduction. As shown in the examples, the instances in each image are close to

each other, and their bounding boxes are overlapped. Without Shape-aware RoIAlign that exploits the mask information for feature extraction, vanilla Mask R-CNN is unable to accurately classify the objects and predict the regressions. By contrast, MR R-CNN successfully separates the features between close objects based on mask inputs, thus is able to produce more accurate outputs.

4.3. Ablation Study

We evaluate our method on COCO 2017 validation sets for ablation study. In order to ensure that the results are stable, all the ablation study experiments are conducted on all the three backbone networks.

4.3.1 Refining module without RoIAlign

Since two novel parts are introduced in MR R-CNN, it is necessary to break down their respective contributions. To this end, we replace the Shape-aware RoIAlign with RoIAlign in MR R-CNN and evaluate its performance.

Backbone	RM SARA	AP_b	AP_m
ResNet-50		37.8	34.2
ResNet-50	✓	38.6(+0.8)	35.0(+0.8)
ResNet-50	✓ ✓	39.5(+1.7)	35.4(+1.2)
ResNet-101		40.1	36.1
ResNet-101	✓	40.5(+0.4)	36.6(+0.5)
ResNet-101	✓ ✓	41.4(+1.3)	37.1(+1.0)
ResNeXt-101		42.2	37.8
ResNeXt-101	✓	42.7(+0.5)	38.3(+0.5)
ResNeXt-101	✓ ✓	43.6(+1.4)	38.8(+1.0)

Table 3: Ablation study results on COCO 2017 validation set to verify the importance of Shape-aware RoIAlign. The ✓ under RM means that the model has a refining module, and the ✓ under SARA means the refining module uses Shape-aware RoIAlign for RoI feature extraction. No ✓ means the vanilla Mask R-CNN model. Every backbone network contains a FPN unless otherwise specified.

As the results shown in Table 3, without Shape-aware RoIAlign, the refining module can outperform the vanilla Mask R-CNN with 0.6 box AP (averaging on three different backbones) and 0.6 mask AP. This is reasonable, since the box predictions generated by the box head is more precise than the RoIs generated by the RPN. Thus, features extracted from the former are better than those extracted from the latter, which lead to the performance improvement. Then, Shape-aware RoIAlign improves the performance by another 0.9 box AP and another 0.5 mask AP.

4.3.2 Classification or bounding box Regression?

Our refining module significantly improves the performance of object bounding box detection. But, it is unclear whether this improvement comes from more accurate object classification or more precise bounding box regression. To make it clear, we conduct two ablation experiments by modifying our MR R-CNN: At the refining box head, (1) only classification is performed and the box regression result from the box head is directly used; (2) only box regression is performed and the classification result from the box head is directly used; We compare the performances of these two variants with the performances of Mask R-CNN and MR R-CNN, and the results are shown in Table 4. The results demonstrate that the improvement caused by refined box regression is larger. This is because the refining box head is guided by mask predictions, which encodes sufficient spatial information for bounding box regression.

Backbone	CLS REG	AP_b	AP_m
ResNet-50		37.8	34.2
ResNet-50	✓	38.3(+0.5)	35.0(+0.8)
ResNet-50		39.1(+1.3)	35.1(+0.9)
ResNet-50	✓ ✓	39.5(+1.7)	35.4(+1.2)
ResNet-101		40.1	36.1
ResNet-101	✓	40.4(+0.3)	36.8(+0.7)
ResNet-101		41.2(+1.1)	37.0(+1.0)
ResNet-101	✓ ✓	41.4(+1.3)	37.1(+1.1)
ResNeXt-101		42.2	37.8
ResNeXt-101	✓	42.7(+0.5)	38.6(+0.8)
ResNeXt-101		43.2(+1.0)	38.5(+0.7)
ResNeXt-101	✓ ✓	43.6(+1.4)	38.8(+1.0)

Table 4: Ablation study results on COCO 2017 validation set to verify how much improvement come from refined object classification and bounding box regression, respectively. The ✓ under CLS means that the refining box head performs object classification, and the ✓ under REG means the refining box head performs box regression. No ✓ means the baseline Mask R-CNN model. Double ✓ means the complete Mask Refining R-CNN model. Every backbone network contains a FPN unless otherwise specified.

α	AP_b	AP_m	α	AP_b	AP_m
0	39.1	35.1	1	39.5	35.4
0.1	39.3	35.2	2	39.5	35.4
0.2	39.3	35.2	5	39.4	35.3
0.5	39.5	35.4	10	39.2	35.2

Table 5: Results for different values of weight α on COCO 2017 validation set. The model is MR R-CNN based on backbone ResNet-50 FPN.

4.3.3 On the weights of refining at inference

At inference, we use α to combine the classification scores in the vanilla Mask R-CNN and our refine module. Here, we conduct ablation study on α , the results of which are shown in Table 5. The results show that the best performance is achieved when α is within the range from 0.5 to 2.

5. Conclusion

The dominant paradigm for instance segmentation is “detect then segment”, while this sequential paradigm struggles when dealing with huddled instances. We found one reason which is the rectangle-based RoI feature extraction strategies used for the detection step that mix features from huddled instances, which makes the detection problem ill-posed.

To address this issue, we proposed a mask-guided RoI feature extracting strategy, named Shape-aware RoIAlign, which focuses feature extraction within a region aligned well with the shape of the instance-of-interest rather than a rectangular RoI. We realized Shape-aware RoIAlign by introducing a refining module built upon Mask R-CNN, which takes the mask predicted by Mask R-CNN as the region to guide the computation of Shape-aware RoIAlign and then updates the box and mask predicted by Mask R-CNN based on the re-computed RoI features. The experimental results on MS-COCO benchmark showed our method achieved a consistent improvement over Mask R-CNN baseline, thanks to feature re-computation by Shape-aware RoIAlign.

References

- [1] Pablo Andrés Arbeláez, Jordi Pont-Tuset, Jonathan T. Barron, Ferran Marqués, and Jitendra Malik. Multiscale combinatorial grouping. In *Proc. CVPR*, pages 328–335, 2014.
- [2] Anurag Arnab and Philip H. S. Torr. Pixelwise instance segmentation with a dynamically instantiated network. In *Proc. CVPR*, pages 879–888, 2017.
- [3] Min Bai and Raquel Urtasun. Deep watershed transform for instance segmentation. In *Proc. CVPR*, pages 2858–2866, 2017.
- [4] Daniel Bolya, Chong Zhou, Fanyi Xiao, and Yong Jae Lee. YOLACT: real-time instance segmentation. In *Proc. ICCV*, 2019.
- [5] Zhaowei Cai and Nuno Vasconcelos. Cascade R-CNN: delving into high quality object detection. In *Proc. CVPR*, pages 6154–6162, 2018.
- [6] Kai Chen, Jiangmiao Pang, Jiaqi Wang, Yu Xiong, Xiaoxiao Li, Shuyang Sun, Wansen Feng, Ziwei Liu, Jianping Shi, Wanli Ouyang, Chen Change Loy, and Dahua Lin. Hybrid task cascade for instance segmentation. In *Proc. CVPR*, pages 4974–4983, 2019.
- [7] Liang-Chieh Chen, Alexander Hermans, George Papandreou, Florian Schroff, Peng Wang, and Hartwig Adam. Masklab: Instance segmentation by refining object detection with semantic and direction features. In *Proc. CVPR*, pages 4013–4022, 2018.
- [8] Liang-Chieh Chen, George Papandreou, Iasonas Kokkinos, Kevin Murphy, and Alan L. Yuille. Deeplab: Semantic image segmentation with deep convolutional nets, atrous convolution, and fully connected crfs. *IEEE Trans. Pattern Anal. Mach. Intell.*, 40(4):834–848, 2018.
- [9] Xinlei Chen, Ross B. Girshick, Kaiming He, and Piotr Dollár. Tensormask: A foundation for dense object segmentation. In *Proc. ICCV*, 2019.
- [10] Yi-Ting Chen, Xiaokai Liu, and Ming-Hsuan Yang. Multi-instance object segmentation with occlusion handling. In *Proc. CVPR*, pages 3470–3478, 2015.
- [11] Jifeng Dai, Kaiming He, Yi Li, Shaoqing Ren, and Jian Sun. Instance-sensitive fully convolutional networks. In *Proc. ECCV*, pages 534–549, 2016.
- [12] Jifeng Dai, Kaiming He, and Jian Sun. Instance-aware semantic segmentation via multi-task network cascades. In *Proc. CVPR*, pages 3150–3158, 2016.
- [13] Jifeng Dai, Yi Li, Kaiming He, and Jian Sun. R-FCN: object detection via region-based fully convolutional networks. In *Proc. NIPS*, pages 379–387, 2016.
- [14] Dumitru Erhan, Christian Szegedy, Alexander Toshev, and Dragomir Anguelov. Scalable object detection using deep neural networks. In *Proc. CVPR*, pages 2155–2162, 2014.
- [15] Ross B. Girshick. Fast R-CNN. In *Proc. ICCV*, pages 1440–1448, 2015.
- [16] Bharath Hariharan, Pablo Andrés Arbeláez, Ross B. Girshick, and Jitendra Malik. Simultaneous detection and segmentation. In *Proc. ECCV*, pages 297–312, 2014.
- [17] Adam W. Harley, Konstantinos G. Derpanis, and Iasonas Kokkinos. Segmentation-aware convolutional networks using local attention masks. In *Proc. ICCV*, pages 5048–5057, 2017.
- [18] Kaiming He, Georgia Gkioxari, Piotr Dollár, and Ross B. Girshick. Mask R-CNN. In *Proc. ICCV*, pages 2980–2988, 2017.
- [19] Zhaojin Huang, Lichao Huang, Yongchao Gong, Chang Huang, and Xinggang Wang. Mask scoring R-CNN. In *Proc. CVPR*, pages 6409–6418, 2019.
- [20] Alexander Kirillov, Evgeny Levinkov, Bjoern Andres, Bogdan Savchynskyy, and Carsten Rother. Instancecut: From edges to instances with multicut. In *Proc. CVPR*, pages 7322–7331, 2017.
- [21] Yi Li, Haozhi Qi, Jifeng Dai, Xiangyang Ji, and Yichen Wei. Fully convolutional instance-aware semantic segmentation. In *Proc. CVPR*, pages 4438–4446, 2017.
- [22] Xiaodan Liang, Liang Lin, Yunchao Wei, Xiaohui Shen, Jianchao Yang, and Shuicheng Yan. Proposal-free network for instance-level object segmentation. *IEEE Trans. Pattern Anal. Mach. Intell.*, 40(12):2978–2991, 2018.
- [23] Tsung-Yi Lin, Piotr Dollár, Ross B. Girshick, Kaiming He, Bharath Hariharan, and Serge J. Belongie. Feature pyramid networks for object detection. In *Proc. CVPR*, pages 936–944, 2017.
- [24] Tsung-Yi Lin, Michael Maire, Serge J. Belongie, Lubomir D. Bourdev, Ross B. Girshick, James Hays, Pietro Perona, Deva Ramanan, Piotr Dollár, and C. Lawrence Zitnick. Microsoft coco: Common objects in context. In *ECCV*, 2014.
- [25] Shu Liu, Jiaya Jia, Sanja Fidler, and Raquel Urtasun. SGN: sequential grouping networks for instance segmentation. In *Proc. ICCV*, pages 3516–3524, 2017.
- [26] Shu Liu, Lu Qi, Haifang Qin, Jianping Shi, and Jiaya Jia. Path aggregation network for instance segmentation. In *Proc. CVPR*, pages 8759–8768, 2018.
- [27] Wei Liu, Dragomir Anguelov, Dumitru Erhan, Christian Szegedy, Scott E. Reed, Cheng-Yang Fu, and Alexander C. Berg. SSD: single shot multibox detector. In *Proc. ECCV*, pages 21–37, 2016.
- [28] Jonathan Long, Evan Shelhamer, and Trevor Darrell. Fully convolutional networks for semantic segmentation. In *Proc. CVPR*, pages 3431–3440, 2015.

- [29] Ping Luo, Guangrun Wang, Liang Lin, and Xiaogang Wang. Deep dual learning for semantic image segmentation. In *Proc. ICCV*, pages 2737–2745, 2017.
- [30] Davy Neven, Bert De Brabandere, Marc Proesmans, and Luc Van Gool. Instance segmentation by jointly optimizing spatial embeddings and clustering bandwidth. In *Proc. CVPR*, pages 8837–8845, 2019.
- [31] Alejandro Newell, Zhiao Huang, and Jia Deng. Associative embedding: End-to-end learning for joint detection and grouping. In *Proc. NIPS*, pages 2277–2287, 2017.
- [32] Pedro H. O. Pinheiro, Ronan Collobert, and Piotr Dollár. Learning to segment object candidates. In *Proc. NIPS*, pages 1990–1998, 2015.
- [33] Pedro Oliveira Pinheiro, Tsung-Yi Lin, Ronan Collobert, and Piotr Dollár. Learning to refine object segments. In *Proc. ECCV*, pages 75–91, 2016.
- [34] Joseph Redmon, Santosh Kumar Divvala, Ross B. Girshick, and Ali Farhadi. You only look once: Unified, real-time object detection. In *Proc. CVPR*, pages 779–788, 2016.
- [35] Shaoqing Ren, Kaiming He, Ross Girshick, and Jian Sun. Faster R-CNN: Towards real-time object detection with region proposal networks. In *Proc. NIPS*, 2015.
- [36] Zifeng Wu, Chunhua Shen, and Anton van den Hengel. Bridging category-level and instance-level semantic image segmentation. *ArXiv*, 1605.06885, 2016.
- [37] Enze Xie, Peize Sun, Xiaoge Song, Wenhai Wang, Xuebo Liu, Ding Liang, Chunhua Shen, and Ping Luo. Polarmask: Single shot instance segmentation with polar representation. *arXiv preprint arXiv:1909.13226*, 2019.
- [38] Ziyu Zhang, Sanja Fidler, and Raquel Urtasun. Instance-level segmentation for autonomous driving with deep densely connected mrfs. In *Proc. CVPR*, pages 669–677, 2016.
- [39] Ziyu Zhang, Alexander G. Schwing, Sanja Fidler, and Raquel Urtasun. Monocular object instance segmentation and depth ordering with cnns. In *Proc. ICCV*, pages 2614–2622, 2015.
- [40] Hengshuang Zhao, Jianping Shi, Xiaojuan Qi, Xiaogang Wang, and Jiaya Jia. Pyramid scene parsing network. In *Proc. CVPR*, pages 6230–6239, 2017.
- [41] Shuai Zheng, Sadeep Jayasumana, Bernardino Romera-Paredes, Vibhav Vineet, Zhizhong Su, Dalong Du, Chang Huang, and Philip H. S. Torr. Conditional random fields as recurrent neural networks. In *Proc. ICCV*, pages 1529–1537, 2015.
- [42] Xingyi Zhou, Jiacheng Zhuo, and Philipp Krähenbühl. Bottom-up object detection by grouping extreme and center points. In *Proc. CVPR*, pages 850–859, 2019.